MONITORING MORPHOLOGY OF THE SAND ENGINE LEESIDE USING ARGUS' cBATHY

Meagan E. Wengrove[1], Martijn Henriquez[2], Matthieu A. de Schipper[3], Rob Holman[4], and M.J.F. Stive[5]

Abstract

The Sand Engine is a mega-nourishment constructed in 2011 with the purpose of replenishing the surrounding southern Dutch coast by exploiting the strength of local alongshore currents for the next 20 years. Long term monitoring of the Sand Engine depends upon remote sensing coupled with in-situ measurements due to both its large spatial and temporal scales and variability. Herein, emphasis is made upon quantitatively and qualitatively observing the effects of this mega-nourishment upon its leeward side in the direction of the predominant alongshore current. One of the first applications of cBathy along the Dutch coast shows promising results for this remote technique to capture morphodynamics within the area over the coming years. cBathy is an algorithm developed to make estimations of nearshore bathymetry based upon the celerity of the propagating wave field extracted from Argus coastal images. So far, analysis shows that the Dutch wave climate variability influences hourly cBathy depth approximations, however running average depth estimations yield small deviation compared with a measured ground truth bathymetry of the area.

Key words: Morphology, Remote sensing, Alongshore currents, Beach nourishment, cBathy, Argus

1. Introduction

In October 2011, the construction of the Sand Engine on the southern Dutch coast was completed. The Sand Engine is a large peninsula of nourished sand positioned in an erosive coastal region (formerly nourished on average every 4 to 5 years) that uses the local alongshore currents to naturally replenish the surrounding coasts (Mulder and Stive, 2011). This innovative pilot, mega-nourishment is designed based upon *Building with Nature* principles where the sediment will be spread along the coast by natural processes over the next 20 years (Stive et al., submitted). *Building with Nature* conceptualizes and advances flexible integration of land and water within the coastal community of The Netherlands (Waterman, 2010).

The Sand Engine currently extends approximately 3 kilometers in the alongshore and reaches 800 m out into the North Sea (Figure 1 shows a map identifying the Sand Engine location). This flexible structure has changed and will evolve in shape and length over the coming years. Thus, an extensive monitoring campaign is presently being undertaken to gain insight into the development of the altered coastal system. The overall long term physical research objective is to evaluate the effects that this nourishment has upon the coastal morphodynamics and hydrodynamics of the area (Stive et al., submitted).

Sediment transport and erosion are processes that determine the morphological dynamics of the nearshore and can be driven by both waves and currents (Beach and Sternberg, 1992). The altered nearshore surrounding the Sand Engine creates energetic hydrodynamic conditions within the proximate coastal region. A mega-nourishment, like the Sand Engine, will have an impact on the hydrodynamics and morphodynamics within the surrounding environment. In addition, this impact will vary in time since the shape of the Sand Engine is dynamic so the hydrodynamics are constantly changing.

Observations of the current hydrodynamic and morphologic conditions as well as an analysis of various remote sensing techniques to monitor the dynamics of the Sand Engine are presented herein. An emphasis is made upon preliminary results showing how cBathy performs on the Southern Dutch coast with altered wave and current conditions compared with Duck, North Carolina, the location where cBathy

[1]Dept. Hydraulic Eng., Delft Univ. of Technology, Stevinweg 1, 2628 CN Delft, NL. m.e.wengrove@tudelft.nl
[2]Dept. Hydraulic Eng., Delft Univ. of Technology, Stevinweg 1, 2628 CN Delft, NL. m.henriquez@tudelft.nl
[3]Dept. Hydraulic Eng., Delft Univ. of Technology, Stevinweg 1, 2628 CN Delft, NL. m.a.deschipper@tudelft.nl
[4]Oceanography, Oregon State Univ., 104 Ocean Admin Bldg, Corvallis, OR, USA. holman@coas.oregonstate.edu
[5]Dept. Hydraulic Eng., Delft Univ. of Technology, Stevinweg 1, 2628 CN Delft, NL. m.j.f.stive@tudelft.nl

was developed and tested (see Holman, et al. 2013). cBathy is an algorithm developed to make estimations of nearshore bathymetry based upon the celerity of the propagating wave field (see Holman, et al. 2013 and Plant, et al., 2008). Monitoring of nearshore morphology is one of the main objectives of the Sand Engine pilot experiment, and the applicability of an almost continuous technique to do so is an important investment to this study.

2. Sand Engine Monitoring Program

There are a wide range of spatial scales and temporal variability that are typical of a nearshore environment; waves, currents, and morphologies can vary widely within the nearshore (Holman and Stanley, 2007). The Sand Engine is dynamic by definition, its size is vast, spanning kilometers, and the pilot mega-nourishment is expected to last for 20 years. The characteristics of the Sand Engine call for remotely sensed monitoring techniques that can capture both large spatial scales and temporal variability over long periods of time (Holman and Haller, 2013). Even so, remote measurements are indirectly related to the quantity of interest, so field verification is required to establish the validity of the measurements and to understand their limitations at this new field site (Perkovic, et al., 2009). Remote monitoring techniques paired with in-situ sampling make for a comprehensive monitoring campaign of this pilot experiment.

Instrumentation to monitor the hydrodynamic and morphodynamic changes around the Sand Engine include: two Argus monitoring stations, Doppler X-band radar, two permanent acoustic Doppler current profilers (ADCP), a directional-waverider wave buoy, regular jet-ski bathymetric surveys; and at times, various temporary monitoring campaign equipment.
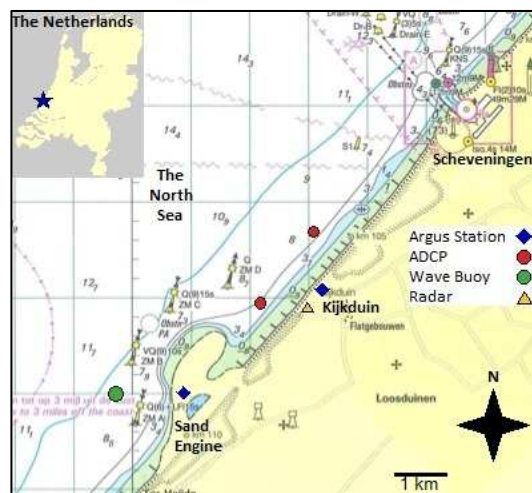

Figure 1: Map showing the location of the Sand Engine in the broader southern coastal region of The Netherlands with instrument locations displayed as colored shapes.

A map demonstrating the relative locations of permanent instrumentation including both Argus stations, the radar (installed June 2012), both ADCPs, and the wave buoy are shown in Figure 1. Of the two Argus stations, one station is positioned on the Sand Engine itself (installed mid-March 2013), and a second station is positioned at Kijkduin (installed end of October 2012), just north of the Sand Engine, as to capture the leeward dynamics in the direction of the dominant alongshore current. The X-band radar is co-located with the Kijkduin Argus station; however, its monitoring window extends into the field of view of the Sand Engine Argus station, and overlaps with the locations of the permanent ADCPs and wave buoy.

The Kijkduin Argus station is composed of six 5-megapixel cameras capable of sampling at 2 Hz with a field of view of approximately 8 km in the alongshore from the Sand Engine to Scheveningen (with a pixel resolution ranging from 0.1 m at station to 50 m at 4 km in either direction) and approximately 1500 m cross shore (with a pixel resolution ranging from 0.1 m at station to 15 m at a cross shore distance of 1500 m). Figure 2 demonstrates an alongshore merged and rectified image of 8 km taken from the Kijkduin Argus station. Already within this image the variability in shoreline, bar line, and Sand Engine shape are apparent. The offshore annual average significant wave height is 1 m coming from the

Northwest with an average significant wave period between 5.4 s and 10.4 s (Wijnberg, 2002). The tidal range at the Sand Engine and Kijkduin is generally 1.4 m (neap) to 1.9 m (spring) (Wijnberg, 2002).
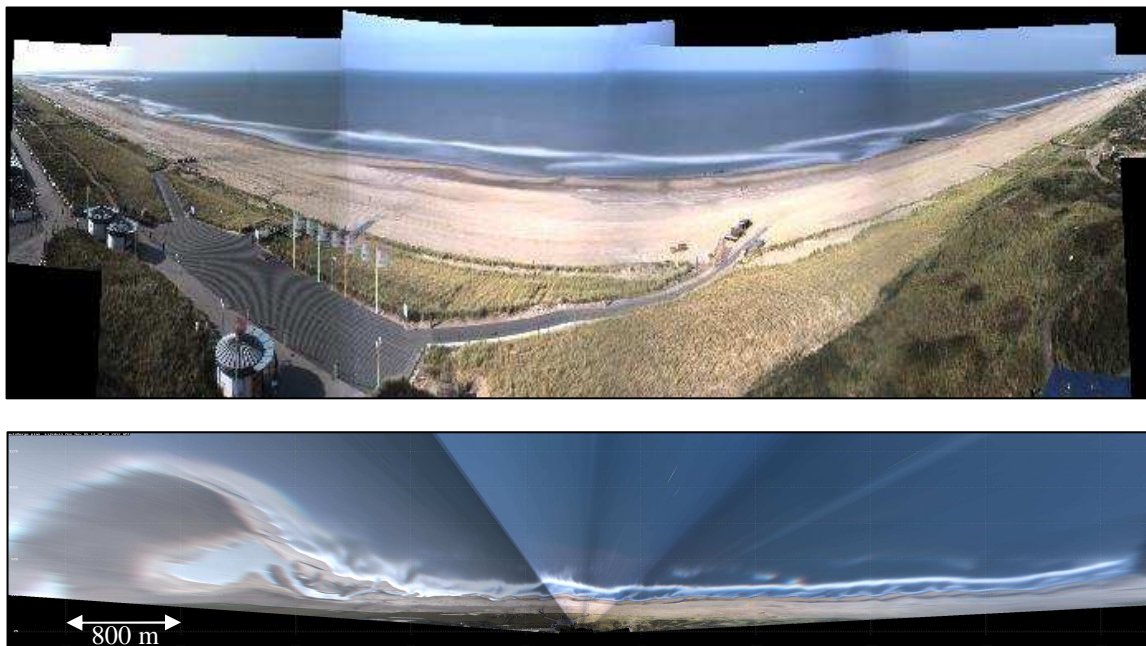

Figure 2: Merged (upper) and rectified (lower) time exposure image capturing leeside of Sand Engine from Kijkduin.

2.1. Monitoring of Hydrodynamics

The ADCPs, wave buoy, and Doppler X-band radar are currently used to monitor the hydrodynamic variability at the Sand Engine. The X-band radar frequency band is most appropriate for near-shore applications, and operates with a rotating antenna to build an image with pixels captured in a serial fashion by pulses transmitted at approximately 2000 Hz, the pulses intersect the ocean surface and the returned echoes are recorded as a function of time of flight, and hence range, out to 1–3 km (Holman and Haller, 2013). Doppler radar has proven to be a viable method to measure nearshore currents (see Perkovic, et al., 2009, Holman and Haller, 2013, and Paduan and Rosenfeld, 1996).

2.1.1. *Application of and basic theory behind SeaDarQ*
In this case, the X-band radar uses SeaDarQ software (see Swinkels et al., 2012) to resolve currents within a large spatial extent surrounding the Sand Engine, the SeaDarQ software was made to measure currents in offshore regions, but compares with reasonable error to the in-situ current data from the ADCPs situated within its viewing window.

The SeaDarQ software package uses the X-band radar data to resolve currents by computing the localization of wave energy determined by the linear current-dispersion relation for waves propagating in shallow water, as defined by,

$$\sigma = \sqrt{gk \tanh(kh)} + uk, \tag{1}$$

where, σ is the radial frequency as defined by $2\pi/T$, T is the wave period, g is the acceleration due to gravity k is the wavenumber magnitude as defined by $2\pi/L$, L is the wave length, h is the depth of the water, and u is the current vector. To apply the linear current-dispersion relation, first, the three dimensional Fourier transform of the re-discretized radar image on a Cartesian grid is calculated and returns the wavenumber and directional spectra. The product of the wavenumber-directional spectra can be used in the linear current-dispersion relation and results as a funnel-shaped spectral energy distribution, where the current vector induces distortion of the radial symmetry of the funnel. The current term, u, in (1) results in a bending of the wave energy in the direction of the current. The amount of distortion increases with wavenumber and the shape of the dispersion relation cone is determined by the current and the water depth

(Kleijweg, et al., 2005 and Holthuijsen, 2007). The SeaDarQ software then returns quality control parameters for its estimations of depth, wave statistics, and currents.

2.2. Monitoring of Morphology

Morphology, more specifically, bathymetry has typically been measured with survey vessels and jet-skis implementing instrumentation such as echo sounders or sonar (Lippmann and Smith, 2009). However, in a large dynamic area that needs more continuous monitoring, video imaging techniques and radar can be used to approximate depth and then these estimations can be verified occasionally with physical bathymetric measurements (Holman, et al. 2013 and Plant, et al., 2008). While radar can also approximate depth, preliminary data shows that the SeaDarQ software being used at the Sand Engine site outputs large relative errors when entering the surf zone and has averaging bins that are too large to detect morphologic features of interest. The surf zone at the Sand Engine is of interest because of its fast morphologic changes and high spatial variability (see Figure 2). Therefore, the method outlined here, cBathy, is currently being applied to data collected from Argus camera systems, but can potentially also be applied to radar data as well (Holman, et al., 2013).

Analysis provides primarily focus upon the Kijkduin Argus station, which monitors the leeward side of the Sand Engine. As stated, the camera station has the capability to sample at 2 Hz, which provides reasonable temporal resolution to facilitate 'time stack' pixel array analysis as outlined in Holman and Stanley (2007). There are various products that use time stack analysis including estimating bathymetry using cBathy as outlined in Holman et al. (2013), and estimating alongshore currents using time stacks (see Perkovic et al., 2009 and Chickadel, et al., 2003).

2.2.1. Application of and basic theory behind cBathy
Water depth can be estimated using the inverse depth approximation using the dispersion relation by rearranging Equation (1) for depth as,

$$h = \frac{1}{k} \tanh^{-1} \frac{(\sigma - u \bullet k)^2}{gk}, \qquad (2)$$

where this equation is a rearranged from of the linear current-dispersion relation.

Assessing the spatial and temporal variations of currents in the nearshore is a critical step into predicting sediment transport and thus the morphological change of the nearshore bathymetry (Perkovic et al., 2009). At this point it is worth noting the types of currents that can affect the celerity or phase speed of wave propagation, where celerity, $c = \sigma/k = L/T$. Alongshore currents do not have a great affect upon the propagation of a wave primarily because it does not, generally, act in the same direction as waves that are propagating into the coast. However, if there is a current flowing in the same direction as the wave propagation, it can increase the phase speed of the wave (Holland, 2001 and Holthuijsen, 2007).

In its current form, cBathy excludes the effects of currents in its depth approximation, and instead uses the linear dispersion relation to find depth from estimated wavenumber for various predefined frequencies,

$$\sigma = \sqrt{gk \tanh(kh)}. \qquad (3)$$

In environments where there is a strong current in the same direction as wave propagation, this approximation will induce error. In the studies of Thornton and Guza (1982), Stockdon and Holman (2000), Holland (2001), Plant et al. (2008), and Holman et al. (2013), each, either measured phase speeds using in-situ data or remotely sensed data and each noted relatively low influence of currents upon phase speeds. For those studies that made inverse depth approximations, the error between remotely sensed and physically measured depths were low. These studies were completed at three separate field sites, including: Torrey Pines Beach near San Diego, CA; Duck, NC; and Agate Beach, OR. Even with results from these three case studies confirming the relatively low influence of currents, validation of depth estimations and consideration of current conditions at each subsequent field site is still necessary.

Now, considering the application of cBathy, before the use of the linear dispersion relation there are several steps between collection of gridded time stacks of pixel intensities and estimating a bathymetry, the entire process is outlined in Holman et al. (2013), and it is appropriate to reference Plant et al. (2008) for further understanding, but a brief summary is given here.

cBathy works by approximating depth from products of temporal spectral analysis and spatial cross

spectral analysis over an array of collected time stacks of pixel intensities. A time stack is a gridded array of pixels collected at predefined coordinates related to wave characteristics of interest over the analysis domain (see Holman et al., 2013 for an example of the spatial layout of a pixel cBathy array). Each pixel in the gridded time stack array is collected for 17 minutes at 2 Hz to yield adequate temporal sampling to perform spectral analysis. The gridded time stack locations should be positioned to include at least five pixels per the shortest wavelength of interest. For example, at the Kijkduin Argus station, the average significant wave period is 5 seconds. Therefore in 1 meter water depth this yields a 12 meter wave length, thus the cross shore pixel spacing needs to be 3 meters (the alongshore spacing was chosen to be a 10 meter spacing to satisfy bathymetric resolution requirements). This pixel spacing calculation relates to the Nyquist wavelength for the wavenumber spectra and is approximated by collecting 5 pixel time stacks per shortest wavelength of interest (see Plant et al., 2008 for discussion related to the Nyquist wavenumber).

After collecting the cBathy time stacks, each time stack of 2048 temporal samples undergoes an FFT, or fast Fourier transform, to transform analysis from the time domain to the frequency domain and determine the spectral energy within each frequency band for each collected pixel time stack. Conceptually, this portion of the analysis will deduce the dominant frequencies of waves passing by a pixel stack due to the physical nature of a wave front generally being visually darker than its back as it approaches the shore. cBathy will only perform analysis and compute wavenumbers for the dominant frequencies within a predefined frequency range. At Kijkduin the predefined frequency range is 1/3 to 1/12 Hz.

For each point in the gridded array cross spectral analysis is used to find phase and coherence of that point compared to adjacent points in subset gridded arrays, or analysis tiles, to allow for faster computation. The analysis tile width and length is also user defined. For each analysis tile the cross spectra are computed for a subset of frequencies surrounding each user specified frequency of relevance. In the case of Kijkduin, the cross spectra are computed using each frequency of relevance as a central frequency of computation from 1/3 to 1/12 Hz. The cross spectra are calculated to infer the related coherence and phase spectra at later steps. The phase and coherence are defined by the cross spectra as,

$$C_{i,j}(f) = \langle \hat{G}^*(x_i, f) \hat{G}(x_j, f) \rangle = \gamma_{i,j,f} \exp(\sqrt{-1}\phi_{i,j,f}), \qquad (4)$$

where, C is the cross spectra of each frequency band, $\hat{G}$ is the normalized FFT of the time series of pixel intensities at each x_i and x_j location, $\hat{G}^*$ is the complex conjugate of $\hat{G}$, γ is the coherence, and ϕ is the phase (see Holman et al. 2013 and Plant et al., 2008). For each cross spectral result the coherence is calculated and the most dominant 4 to 6 frequencies (based upon user definition, Kijkduin case uses 6) are kept for further analysis. The coherence is an indicator of when the associated phases are trustworthy. In this analysis the wave number used to infer depth is computed from the slope of the phase ramp of the phase spectra, therefore coherent phases are very important, so only the 4 to 6 most coherent frequencies are kept for each analysis point in the gridded array. It is worthwhile to note that each analysis point over the entire array does not necessarily have the same dominant frequencies as to eventually approximate a bathymetry.

To estimate the wave number, empirical orthogonal function (EOF) of the cross spectra are used for each of the dominant frequencies to eliminate the possibility of analyzing multiple, directionally-spread wave trains in any frequency band. From the phase spectra, and the wave number, k, is defined in as the slope of the phase ramp,

$$k(x_{i,j}, f) = \frac{d\phi_{i,j,f}}{dx_{i,j,f}}, \qquad (5)$$

where, k is the wave number (Merrifield and Guza, 1990, Stockdon and Holman, 2000). However, in cBathy, the wavenumber and wave angle are computed using the decomposed eigenvectors (v) from the cross spectra of each dominant frequency where the associated eigenvalue (λ) is used as a quality control parameter for the associated dominant frequency result. In the EOF analysis correlation matrix, the eigenvectors correspond to the principle components and the eigenvalues correspond to the variance explained by the principle components, so the largest eigenvalues relate to principle components associated with most of the convertibility among the observed data (Bendat and Piersol, 2000). This complex decomposition defines the optimum wavenumber and, wave direction by the best match between the observed and the modeled spatial phase structure. Where the modeled spatial phase structure relates the eigenvector to the wave length, wave angle and arbitrary phase shift (free parameter). The best fit of the forward model to the EOF eigenvectors is found using the Levenberg-Marquardt algorithm of the computational program Matlab. During the procedure, weighting is applied using a Hanning filter to the EOF eigenvectors of the analysis tile to focus weight around the analysis point. The skill of the fit and the

eigenvalue of the first EOF are used as quality criteria of the estimated wavenumber. The whole procedure will result in a number of predicted wavenumbers for the surviving frequencies.

Finally, the linear dispersion relation, Equation (3) can be used to approximate depth with a known wavenumber and frequency for each of the 4 to 6 dominant frequencies. Now there are 4 to 6 approximations of depth, due to the 4 to 6 chosen dominant frequencies. The final depth comes from the best weighted fit of the dispersion relation (Equation 3) to the wave numbers and frequencies using the Levenberg-Marquardt algorithm. Weights are based on the previous mentioned skill, the eigenvalue of the EOF and distance between i and j (see Holman et al., 2013). The aforementioned analysis is completed for each time stack collected and is referred to as hourly cBathy analysis for the rest of this paper.

Subsequently, cBathy hourly results are assimilated by a running average Kalman filter that uses a user defined confidence parameter to weight the influence of new hourly depth approximations compared to the current running average depth approximation up until the newest result, this running average can be computed for as long as cBathy results are available (see Holman et al., 2013).

3. Brief Overview of Hydrodynamics at Kijkduin

The southern coastal currents of The Netherlands are traditionally fairly unidirectional alongshore currents, flowing northeast with flood tide and southwest with ebb tide, where the dominant alongshore current flows northeast. During flood tide, observationally, the current fields resolved from the X-band radar show that the Sand Engine creates an alongshore flow obstruction, where the fastest velocities occur at the tip protruding into the North Sea. This hydrodynamic characteristic creates a leeward shadow and differences in flow velocities of approximately 0.15 m/s over 1 to 2 km. The leeward shadow has the potential to create many interesting current fields, where Figure 3 shows tidally phase averaged current fields for flood tide, ebb tide, and a period in the tidal cycle where the leeward shadow is evident. Overall observation shows that dominant current is alongshore, but there is potential for multi-directional currents, especially on the leeward side of the Sand Engine such that current patters may have an impact on local morphodynamics. Figure 3 also shows a comparison of an in-situ ADCP with the radar current vector field. The ADCP velocity magnitude and direction match those of the radar vectors within approximately +/- 0.05 m/s and +/- 5°, respectively.
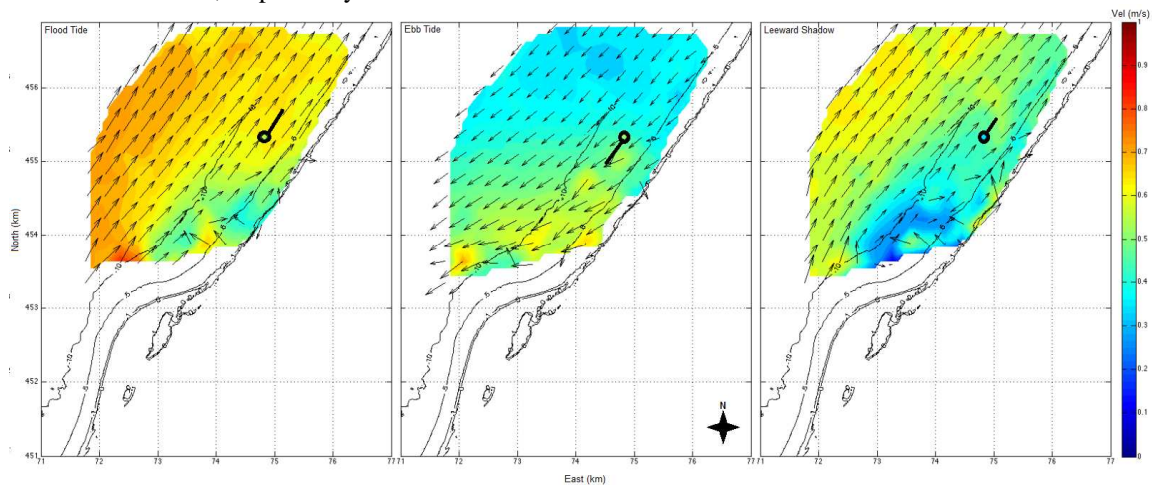

Figure 3: Tidally phase averaged current fields from X-band radar. Left panel shows phase averaged flood tidal current, middle panel shows phase averaged ebb tidal current, and right panel shows a tidally phase averaged leeward shadow during flood tide. Color represents velocity magnitude from 0 m/s (blue) to 1 m/s (red) for both radar vector field and corresponding color of ADCP location point. Vectors show the local magnitude and direction of the velocity vector, and vector magnitude is represented by corresponding underlying color.

4. Analysis of cBathy Performance at Kijkduin

The Argus station at Kijkduin is tasked with ongoing monitoring of the evolving morphodynamics over a large spatial and temporal window. The first cBathy results were collected in mid-February of 2013, and

continuous collection is underway. The cBathy spatial window is 3 km alongshore and 500 m out into the North Sea from the shoreline (see Figure 4). The first ground truth survey of the leeward side of the Sand Engine was collected the first week of March 2013.

4.1. cBathy Kalman Filter Analysis

Using Kalman filtering of cBathy depth estimations over the three weeks prior to the ground truth survey, demonstrate that cBathy is able to well resolve many coastal features, such as sand bars, the foreshore nourishment (at cross shore location of approximately 600 m), and interesting 'pot hole' characteristics close to Sand Engine (see Figure 5). The largest differences between the cBathy approximation and the ground truth survey depths occur at: depths greater than 5 meters, within the deep 'pot hole' features near the Sand Engine at alongshore location between 500 and 1000 m, within the northeast camera window, and at camera intersections. In Figure 5, difference indicated by white shows a 30 cm error window where cBathy performs the best. A difference skewed towards the blue side of the color spectrum indicates an under-prediction of depth by cBathy, and towards red indicates an over-prediction of depth by cBathy. Note that the coastline is at cross shore location of approximately 250 M NAP (Normaal Amsterdams Peil).
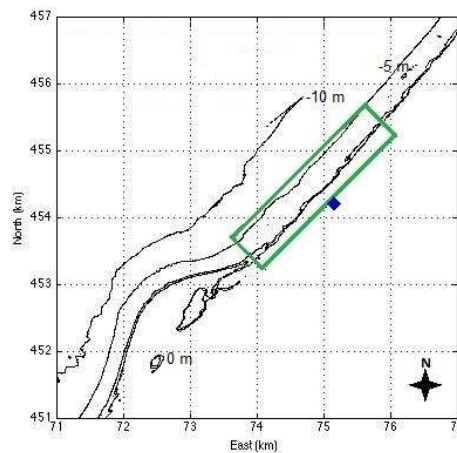

Figure 4: Sand Engine and leeward side coastal bathymetry with overlay of cBathy sampling spatial window outlined in green with Kijkduin Argus station location shown as purple blue diamond.

Cross shore transects spaced every 250 m from -1250 m to 1250 m in the alongshore demonstrate that cBathy Kalman filter depth estimates are visually more accurate to the ground truth measurements in alongshore ranges between -750 m and 750 m away from the Kijkduin Argus station (see Figure 6). Furthermore, the depths estimated to the southwest of the Kijkduin Argus Station, towards the Sand Engine (0 to 1500 m), show less variance between cBathy and ground truth bed elevations than those towards the northeast. Generally, cBathy is able to approximate position and partial bed height deviations of various nearshore features. However, if cBathy does yield error from ground truth, it is usually on the side of a shallow estimation of depth.

4.2. Hourly cBathy Analysis

So far, presented analysis is from Kalman filter running average depth estimates, which consider the previous bed elevation calculated by cBathy when estimating a subsequent bed elevation. This filter is valuable to mitigate large errors in the current hourly cBathy depth estimates. Therefore the Kalman filter also takes into account user input for likelihood of change in the bed elevation over time, as to weight
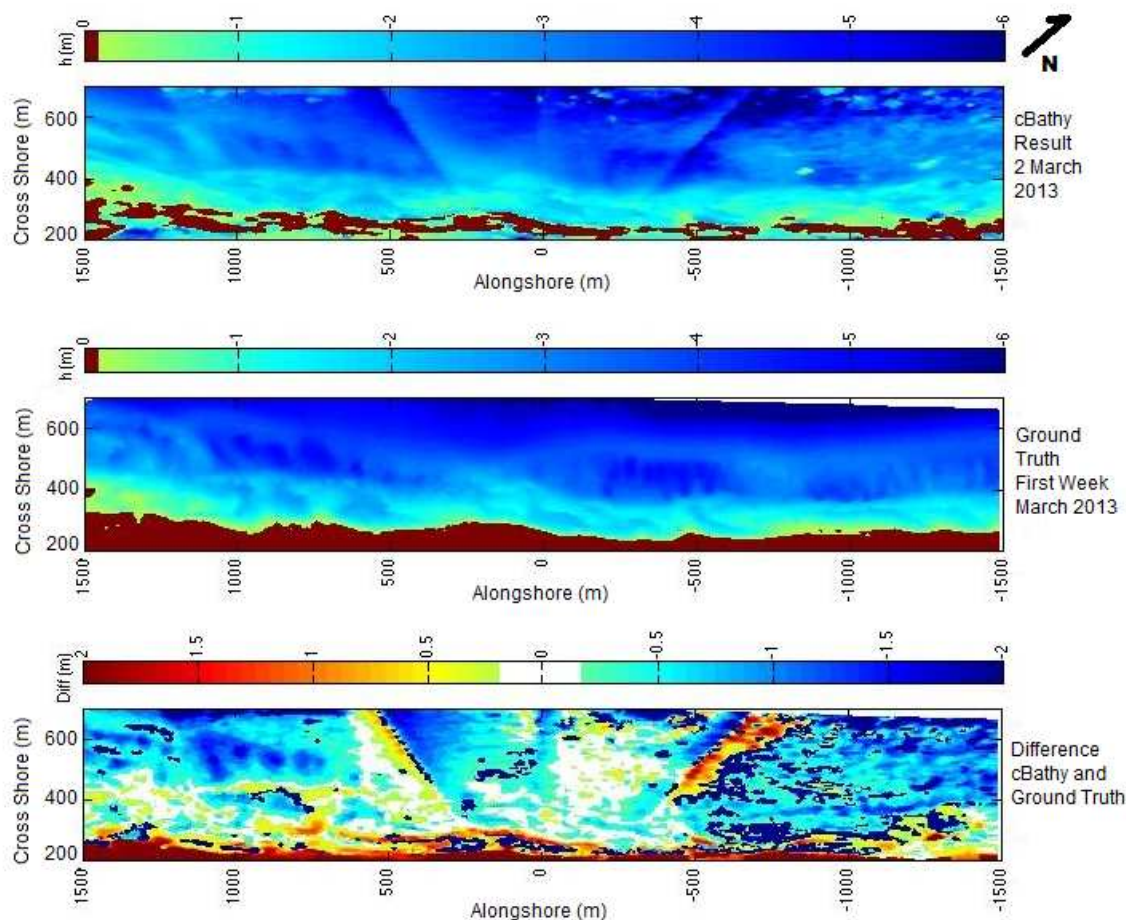
Figure 5: cBathy Kalman filtered depth estimate from 2 March 2013 (upper panel), ground truth bathymetry measurement (middle), and difference between ground truth and cBathy estimate (lower panel). For spatial reference, all alongshore and cross shore distances are plotted relative to the Kijkduin Argus station, where the shore line is located at approximately 250 m on the cross shore scale. Alongshore, the Sand Engine is located southwest of the Kijkduin Argus sampling window, and the Sand Engine is seen at alongshore positions between 1500 m and 500 m. The arrow above the upper panel indicates a cardinal direction of North.
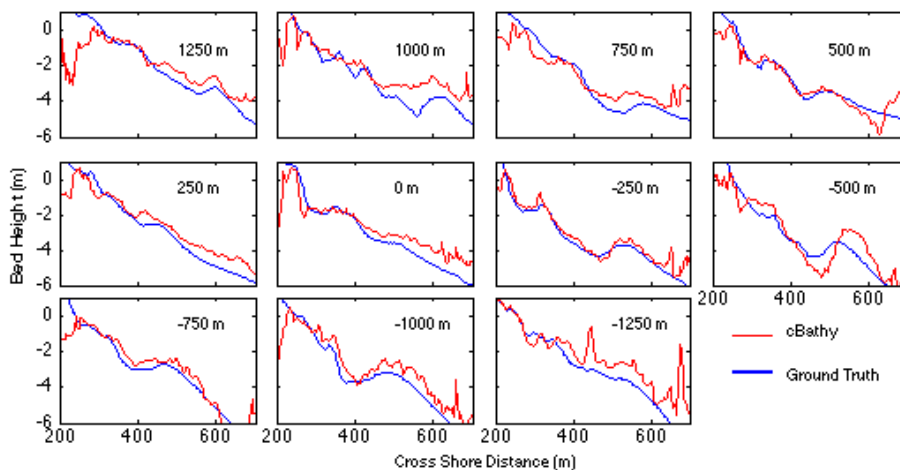

Figure 6: Cross shore transects of cBathy depth estimate (red) compared with ground truth depth estimate (blue). Alongshore distance is shown in upper right hand corner of each plot. Shore line is at approximately 250 m NAP.
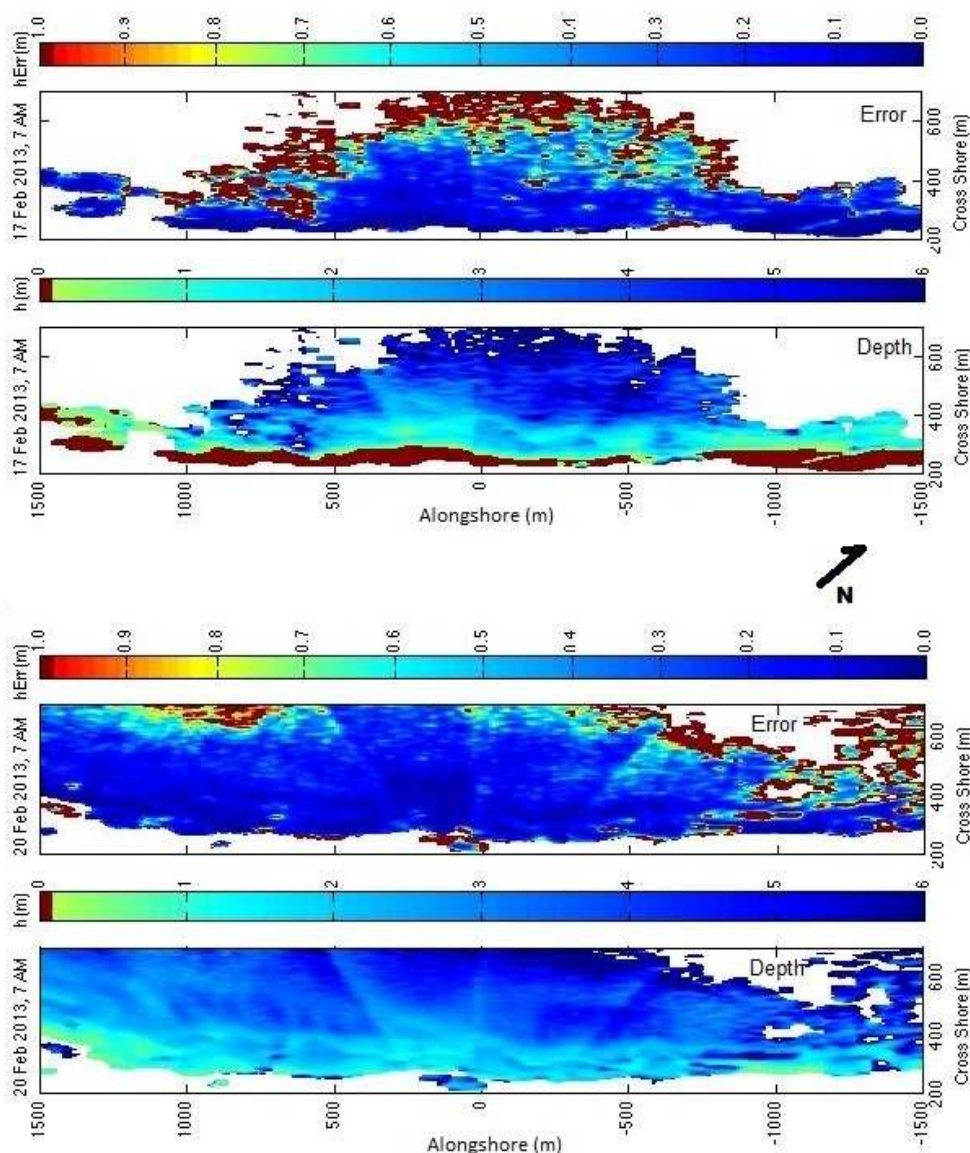
Figure 7: Hourly cBathy depth approximations and associated internally calculated error (not compared to ground truth survey), without Kalman averaging, where top panels show average inversion results (17 Feb 2013, 7 AM), and bottom panels show good inversion results (20 Feb 2013, 7 AM).

Table 1: Wave parameters and associated error with cBathy results in Figure 7

Parameter	17 Feb 2013 7 AM	20 Feb 2013 7 AM
Wave Characteristics at 10 m waterdepth		
H_{max} (cm)	30	106
$H_{1/3}$ (cm)	22	64
T_{max} (s)	18.1	12.63
$T_{1/3}$ (s)	8.5	5.8
Wave direction from North (°) [where 330° is shore normal]	308	355
Wave Spread (°)	43	28
Error and goodness of fit parameters of hourly cBathy estimates		
Bias to Ground Truth (m)	-0.50	-0.18
RMSE to Ground Truth (m)	1.27	1.01
Normalized λ (internal parameter)	11.08	16.38
% NaN Returned, not including shore	47 %	9 %

whether potential large deviations are error induced or actual morphologic variability. The Kalman filter does produce reasonable running averaged depth estimates at Kijkduin. However, it is interesting to consider how various wave climates and current interactions can independently skew hourly cBathy depth estimates.

An example of an average and very good hourly estimates of bathymetry from cBathy and its corresponding internal cBathy algorithm depth error, which relates to the 95% confidence interval of certainty compared to modeled results but not based upon the ground truth survey data, are shown in Figure 7. It is valuable to understand the limitations of cBathy depth estimates aside from sporadic image quality issues, due to sun glare, or rain drops, or fog. Other possibilities for poor depth estimates are mainly attributed to characteristics of the wave field or current field. This could be variance in wave height, wave period, and wave direction and spread. Another interesting feature of the Dutch wave climate is very short wave periods, which is not generally a characteristic of Duck, North Carolina where cBathy was developed. Therefore, an initial objective of analysis of cBathy at Kijkduin is to assess its performance in a different wave climate.

To determine the most plausible sources of error to these hourly cBathy depth approximations, four metrics of data quality are assessed for measures of wave height, wave direction and spread as going towards the coast taken from North, and wave period. In Duck, North Carolina wave height was found to influence cBathy depth approximations the most (Holman et al., 2013). For this analysis the ground truth bathymetry measurement taken during the first week of March 2013 is used as the ground truth for both the 17 Feb. 2013 7 AM estimate as well as the 20 Feb. 2013 7 AM estimate to assess data quality and goodness of fit using the error metrics of bias (calculated as the average of the difference between the cBathy result and the ground truth survey bathymetry) and root mean square error (RMSE). Using the same ground truth for both analyses could induce error because the bathymetry most likely slightly changed between the two estimates and the time of the ground truth survey, however there were not any major storms between 17 Feb and the ground truth survey, so the ground truth is assumed to be reasonable for first approximations of induced error.

Aside from bias and RMSE, which indicate error between the ground truth and hourly cBathy estimates, the associated normalized eigenvalue (λ) and percentage of NaNs returned for hourly estimate are used to assess data quality from the shoreline at 250 m in cross shore distance to the furthest collected analysis points at 700 m cross shore distance. The eigenvalue indicates the amount of variance described over the cBathy analysis tile, and when averaged, over the entire array. The higher the eigenvalue indicates that the eigenvectors more strongly describe the variance in the data, and associated estimates of wavenumber and wave direction are stronger. Bias, RMSE and λ do not account for NaNs in the data set; therefore percentage of NaNs returned is also a valid indicator, where relative error in cBathy estimates are filtered throughout the data processing indicated by λ less than 8 and skill less than 0.5 when assessing the fit of the data to the forward model, anything under these limits are excluded from further analysis and are indicated by NaN return and shown in white in Figure 7. Table 1 compares these error assessments to associated wave heights, directions, and periods from the hourly cBathy depth estimates shown in Figure 7.

Comparing the qualitative results of Figure 7 with the quantitative results of Table 1, the 20 Feb 2013 7 AM results show smaller RMSE and bias, higher λ and less % NaN returned for the overall data set when compared with the 17 Feb 2013 7 AM data indicating that the 20 Feb 2013 7 AM results are of higher quality and fit the ground truth survey more closely. The 20 Feb 2013 7 AM data were taken at mid-rising tide, and the 17 Feb 2013 7 AM data were taken at high-rising tide. The wave statistics show that the significant wave height was smaller for the 17 Feb 2013 7 AM results compared with the 20 Feb 2013 7 AM results, which could affect the data quality and would be consistent with cBathy error analysis in the Duck, North Carolina results (Holman et al., 2013). However, the wave period for the 20 Feb 2013 7 AM data was shorter than that for the 17 Feb 2013 7 AM results; this is an unexpected result, preliminarily demonstrating that good data quality can be obtained from shorter wave periods. Finally, the wave direction for the 17 Feb 2013 7 AM hourly analysis came from the Southwest with a larger spread than those on the 20 Feb 2013 7 AM hourly analysis which came from the North. In this case wave direction and spread could also impact hourly depth estimates. Further environmental factor induced error will continue to be analyzed.

4. Conclusions

The Sand Engine is a dynamic pilot mega-nourishment that is influencing the hydrodynamics and morphodynamics of the surrounding coastal area of The Netherlands. From this preliminary analysis, it is evident that there are many aspects of this mega-nourishment that are potentially interesting. Various tools, instruments, and methods of analysis will continuously provide support to ongoing research around the Sand Engine and are valuable to understanding its continuous evolution. The X-band radar, ADCP, and wave rider buoy are already showing varying current patterns and influence of the Sand Engine on local hydrodynamics, while Argus monitoring provides a continuous data source for qualitatively and quantitatively monitoring the dynamics of the area and will provide insight into how this pilot experiment migrates and develops.

Overall, the performance of cBathy at the Kijkduin Argus station produces quality results; the algorithm is able to resolve many of the characteristic bathymetric features with relatively low qualitative deviation from ground truth bathymetric measurements, especially when employing Kalman filtering. The hourly performance of cBathy in the Kijkduin hydrodynamic climate is potentially influenced by wave characteristics of the domain. There may be other influential factors, such as the complex current environment that skew depth estimates or limit performance, which is left to future analysis. The fundamental background around monitoring the effects of the Sand Engine on the southern Dutch coast make employing a technique such as Argus monitoring and cBathy valuable because of the large temporal and spatial constraints of the project.

Acknowledgements

References

Beach, R. A., and R. W. Sternberg, 1992. Suspended sediment transport in the surf zone: Response to incident wave and longshore current interaction, *Marine Geology*, 108(3a^"4), 275 – 294, doi:10.1016/0025-3227(92)90201-R.

Bendat, J., and A. Piersol, 2000. *Random Data: Analysis and measurement procedures*, 3rd ed., Wiley-Intersci., N.Y.

Chickadel, C. C., R. A. Holman, and M. H. Freilich, 2003. An optical technique for the meganourishment of longshore currents, *Journal of Geophysical Research: Oceans*, 108(C11), 3364, doi:10.1029/2003JC001774.

Holland, T, 2001. Application of the linear dispersion relation with respect to depth inversion and remotely sensed imagery, *Geoscience and Remote Sensing*, 39(9), 2060–2072, doi:10.1109/36.951097.

Holman, R., and M. C. Haller, 2013. Remote sensing of the nearshore, *Annual Rev. of Marine Science*, 5(1), 95–113.

Holman, R., and J. Stanley, 2007. The history and technical capabilities of Argus, *Coastal Engineering*, 54, 477 – 491.

Holman, R., N. Plant, and T. Holland, 2013. cBathy: A robust algorithm for estimating nearshore bathymetry, accepted by *Journal of Geophysical Research*.

Holthuijsen, L, 2007. *Waves in oceanic and Coastal Waters*, Cambridge University Press.

Kleijweg J, G van Vledder & T Steeghs 2005. Integration of X-band remote sensing and numerical modeling of waves.

Lippmann, T., and G. Smith, 2009. Shallow surveying in hazardous waters, *U.S. Hydro*, (1-11).

Merrifield, M. A., and R. T. Guza, 1990. Detecting propagating signals with complex empirical orthogonal functions: A cautionary note, *J. Phys. Oceanography.*, 20, 1628–1633.

Mulder, J.P.M and Stive, M.J.F., 2011. Zandmotor (sand motor): building with nature, *ICDC Conference Proceeding*.

Paduan, J. D., and L. K. Rosenfeld, 1996. Remotely sensed surface currents in Monterey Bay from shore-based HF radar (coastal ocean dynamics application radar), *Journal of Geophysical Research: Oceans*.

Perkovic, D., T. Lippmann, and S. Frasie, 2009. Longshore surface currents measured by Doppler radar and video PIV techniques, *Geoscience and Remote Sensing, IEEE Transactions on*, 47(8), 2787–2800.

Plant, N., K. Holland, and M. Haller, 2008. Ocean wavenumber estimation from wave- resolving time series imagery, *Geoscience and Remote Sensing, IEEE Transactions on*, 46(9), 2644–2658.

Stive, M.J.F., Ranasinghe, R., Luijendijk, A.P., de Schipper, M.A., Aarinkof, S.G.J., and van Gelder-Maas, C., 2013. A new alternative to saving our beaches from sea level rise: The Sand Engine, *Coastal Engineering, submitted.*

Stockdon, H. F., and R. A. Holman, 2000. Estimation of wave phase speed and nearshore bathymetry from video imagery, *Journal of Geophysical Research: Oceans*, 105(C9).

Swinkels, C., H. Peters, and J. van Heesen, 2012. Analysis of current patters in coastal areas using X-band radar images, *Coastal Engineering*.

Thornton, E. B., and R. T. Guza, 1982. Energy saturation and phase speeds measured on a natural beach, *Journal of Geophysical Research: Oceans*, 87(C12), 9499–9508.

Waterman, R.E., 2010. *Integrated Coastal Policy via Building with Nature.* Delft University of Technology.

Wijnberg, K. M., 2002. Environmental controls on decadal morphologic behavior of the Holland coast, *Marine Geology*, 189, 227 – 247.